Superconductivity above 12 K with possible multiband features in CsCl-type PbS

He Zhang [1,2,*] Wei Zhong,[3,*] Yanghao Meng,[1,2,*] Binbin Yue,[3,†] Xiaohui Yu,[1,2,4,‡]
Jian-Tao Wang,[1,2,4] and Fang Hong [1,2,4,§]

[1]*Beijing National Laboratory for Condensed Matter Physics, Institute of Physics, Chinese Academy of Sciences, Beijing 100190, China*
[2]*School of Physical Sciences, University of Chinese Academy of Sciences, Beijing 100190, China*
[3]*Center for High Pressure Science and Technology Advanced Research, 10 East Xibeiwang Road, Haidian, Beijing 100094, China*
[4]*Songshan Lake Materials Laboratory, Dongguan, Guangdong 523808, China*

Binary metal sulfides are a large material family with distinct physical behavior. Here, we report the superconductivity observed in PbS by means of pressure engineering. PbS undergoes a series of electronic phase transitions upon compression, and superconductivity occurs above 23.9 GPa in the high-pressure CsCl-type cubic phase. Further compression suppresses the superconductivity while the T_c is reduced from $\sim$12.0 K at 23.9 GPa to 6.8 K at 44.3 GPa. Marginally higher $T_c \approx 12.3$ K is observed at 19.1 GPa during pressure release. The magnetic field effect verifies the superconductivity with possible multiband features. It is noted that PbS is one of the few binary metal sulfide superconductors with a T_c above 10 K. This work demonstrates that PbS has a high T_c under a moderate pressure due to the chemical "precompression" effect, which is very close to the T_c in pure sulfur at $\sim$100 GPa. PbS also shows unexpected multiband behavior in the cubic structure, benefiting the study of pressure-induced superconductivity and the underlying mechanism in metal sulfide compounds.

I. INTRODUCTION

Element superconductors have been an important research topic in recent decades. Most elements can be superconductors (SCs) at ambient or high pressure, extending the scope of superconductors and enriching our understanding of the superconductivity mechanism [1–3]. Among them, the SC with the highest T_c is expected to be metallic hydrogen, which theoretical calculations predict to be a room temperature SC above at least 400 GPa [4–7]. Otherwise, metallic elements generally have a higher T_c, and the latest high-pressure studies show that Ti has a record-high T_c, reaching 23.6 K at 145 GPa [8] or 26.2 K at 248 GPa [9]. Among the nonmetal elements, sulfur has the highest T_c beyond hydrogen [1], reaching 15 K at 100 GPa [10], while an ac magnetic susceptibility measurement suggests a potentially higher $T_c \approx 17$ K above 157 GPa [11] or 17.3 K at 200 GPa [12].

It is worth noting that the SCs elements with high T_c only exist under ultrahigh pressure conditions (>100 GPa), and even the metallization of pure hydrogen has not yet been achieved experimentally due to the high critical pressure, let alone superconducting hydrogen [7]. However, achieving high T_c SCs by chemical doping or precompression is quite promising. Recently, chemical doping and high pressure helped to stabilize the hydrogen atomic network to be a SC with a T_c close to room temperature, such as H_3S and LaH_{10}, which

reduces the critical pressure on a large scale [13–16]. Motivated by this idea, we planned to achieve a relatively high T_c SC transition in sulfur at a moderate pressure using chemical doping or precompression. We chose sulfur because it has the highest T_c among the nonmetal elements, bar hydrogen.

Although numerous research works on the binary metal sulfide SCs [17–30] have been conducted over recent decades, as shown in Fig. 1, most of their initial motivations differ from this work. At ambient pressure, FeS, 2H-NbS$_2$, NbS$_3$ are representative compounds showing superconductivity, and their T_c values are 5, 6, and 2.15 K, respectively [19,23,31]. Under pressure, the pristine non-SC binary metal sulfide compounds start to show superconductivity and other emergent phenomena as well, such as charge density wave (CDW). Among them, MS_2 and MS_3 ($M = $ metal) are two sets of typical material families in which the SC and CDW show competing or coexistence behavior [22,24,32]. The highest T_c in binary metal sulfides is observed in 2H-TaS$_2$ (16.4 K at 157.4 GPa) [22] or MoS$_2$ (12 K at 200 GPa) [21]. However, no zero-resistance state is presented in 2H-TaS$_2$ and MoS$_2$ at the pressure where the maximum T_c is observed [21,22]. The main reason may be the worse hydrostatic pressure environment at such high pressures. For other SCs in binary metal sulfides, though the target pressure for the T_c maximum of the SC transition is much lower than those in 2H-TaS$_2$ and MoS$_2$, the T_c values are relatively low. None exceed 10 K. Therefore, is it possible to find a binary metal sulfide compound showing a high T_c (above 10 K) at moderate pressure?

Here, we report the superconductivity in the high-pressure cubic phase of PbS. Earlier studies have revealed the structural phase transitions of PbS under pressure. Below 50 GPa, PbS

---

*These authors contributed equally to this work.

†yuebb@hpstar.ac.cn
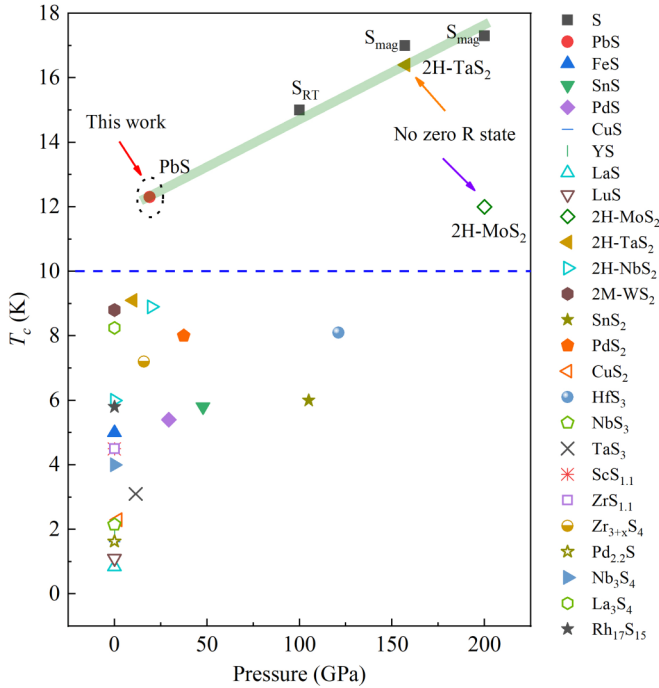
‡yuxh@iphy.ac.cn

§hongfang@iphy.ac.cn

174502-1

FIG. 1. The T_c-P chart for binary metal sulfide superconductors [17–30] and pure sulfur [10–12]. The T_c of S_{RT} is from the temperature-dependent resistance measurement, while the T_c values of S_{mag} are from the low-temperature magnetic susceptibility measurement.

will experience two phase transitions. The first one is around 2.1–2.6 GPa from the original NaCl-type cubic phase (B1 phase) to an orthorhombic phase [33,34], and the second is around 21.1–23 GPa from the orthorhombic phase to a CsCl-type cubic phase (B2 phase) [34–36]. The accurate structure of the intermediate orthorhombic phase is still controversial and highly dependent on the characterization methods and starting sample [33–36]. Meanwhile, Timofeev *et al.* reported the SC transition in PbS and found a $T_c = 6.3$ K with a force load on a diamond-anvil cell, while the actual pressure was not well resolved [37]. In this work, the electrical transport properties of PbS single crystal were investigated in the standard four-probe geometry using the latest high-pressure techniques. The transport behavior change under pressure is consistent with the structural phase transitions. A clear picture is provided to demonstrate the superconductivity in PbS. The highest T_c reaches 12.3 K at 19.1 GPa, and the SC in PbS shows some multiband behavior features. PbS is one of the few binary metal sulfide SCs with a T_c above 10 K, while its critical pressure is much lower.

II. EXPERIMENTAL AND CALCULATION METHODS

The PbS single crystal was synthesized by the chemical vapor transport method. High-purity Pb and S powders were mixed by 1:1 stoichiometric ratio, and sealed in a quartz tube with high vacuum. Then the powder mixture was heated at $850°$ C at one side of the tube and single crystal was then formed at $500°$ C at the other side.

The temperature-dependent electrical resistance of PbS single crystal under high pressure was measured via the standard four-probe geometry in a commercial cryostat (Janis Research) from 1.7 to 300 K by a Keithley 6221 current source and a 2182 A nanovoltmeter. A BeCu alloy diamond-anvil cell with two opposing 300-μm culet anvils was used to generate high pressure. A thin flake was cut from the bulk crystal along the easy exfoliation direction, and a small piece of the sample was loaded into the sample chamber in a rhenium gasket with c-BN insulating layer. Four Pt electrodes were placed onto the surface of the samples in the chamber. KBr was used as the pressure medium. Finally, a ruby ball was loaded to serve as an internal pressure standard. The high-pressure Raman spectra were collected using a Renishaw micro-Raman spectroscopy system equipped with a second-harmonic Nd:YAG laser, and silicon oil was used as pressure medium. A 532-nm laser was used, with a spot size of 1–2 μm. A pair of low fluorescent diamonds was used for Raman measurement. The laser power was maintained at a relatively low power level to avoid overheating during measurements. *In situ* high-pressure ultraviolet-to-visible-to-near-infrared (UV-VIS-NIR) absorption spectroscopy was performed on the home-designed spectroscopy system (Ideaoptics, Shanghai, China). The high-pressure infrared experiments were performed at room temperature on a Bruker VERTEX 70v infrared spectroscopy system with a HY-PERION 2000 microscope. The spectra were collected in transmission mode in the range of $600-8000\,cm^{-1}$ with a resolution of $4\,cm^{-1}$ through an $\sim 50{\times}50\,\mu m^2$ aperture. KBr was used as pressure medium for UV-VIS-NIR and infrared spectroscopy measurements.

Our density functional theory calculations are performed using the Vienna *ab initio* simulation package [38] with the projector augmented wave method [39]. The Perdew-Burke-Ernzerhof revised for solids [40] exchange correlation functional is adopted for the evaluation of structural and electronic properties of B2-type PbS under pressure. The valence states $5d^{10}\,6s^2\,6p^2$ for Pb and $3s^2\,3p^4$ for S are used with the energy cutoff of 800 eV for the plane-wave basis set. The Brillouin-zone sampling is performed using a $20{\times}20{\times}20$ k-point grid for the total energy and electronic band structure calculations. The electronic density of states (DOS) is calculated using the Gaussian smearing with a broadening energy of 0.1 eV and 4000 grid points on which the DOS is evaluated. Convergence criteria employed for both the electronic self-consistent relaxation and the ionic relaxation are set to 10^{-8} eV and 0.01 eV/Å for energy and force, respectively. In the B2-type PbS crystal structure, the Pb and S atoms occupy the $1a$ (0.0, 0.0, 0.0) and $1b$ (0.5, 0.5, 0.5) Wyckoff positions, respectively. The lattice parameters are calculated to be 3.341, 3.275, 3.222, and 3.179 Å under 20, 30, 40, and 50 GPa, respectively.

III. RESULTS AND DISCUSSION

PbS is a NaCl-type B1 phase at ambient pressure, a semiconductor with a small band gap of 0.42 eV [41]. As shown in Fig. 2, the transport measurement at 1.1 GPa shows a typical semiconducting behavior. Further compression enhances the semiconducting behavior. The resistance is too
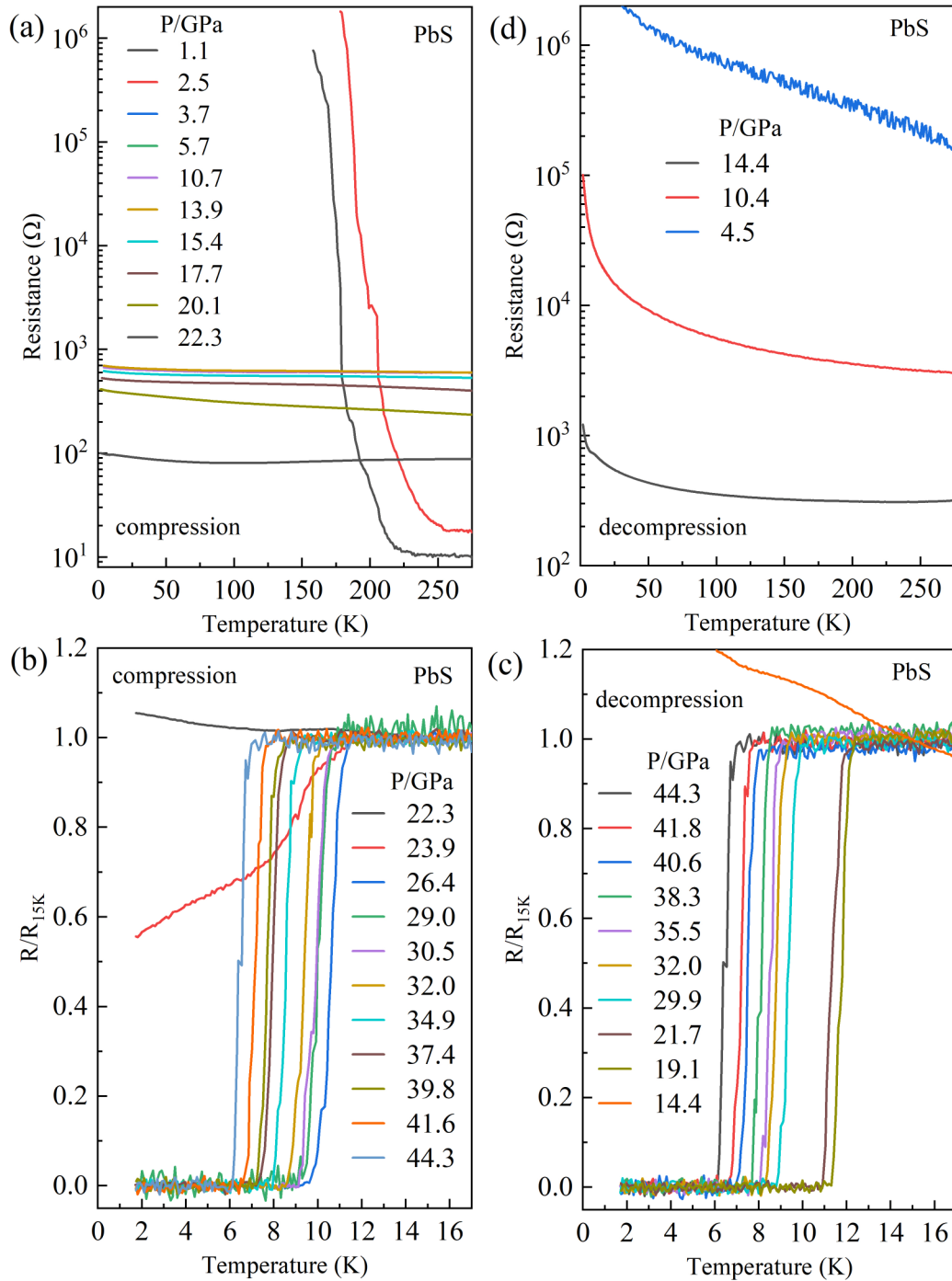
FIG. 2. The electrical transport behavior of PbS under pressure. (a) The R-T curves from 1.1 to 22.3 GPa upon compression; (b) the normalized R-T curves from 22.3 to 44.3 GPa upon compression; SC occurred above 23.9 GPa; (c) the normalized R-T curves from 44.3 to 14.4 GPa during the decompression process; (d) the R-T curves from 14.4 to 4.5 GPa during decompression; the SC transitions disappeared, and the sample returned to an insulating state.

large to be measured above 2.5 GPa, consistent with the structural phase transition from the low-pressure B1 phase to the intermediate orthorhombic phase [33,34,36,42]. Previous resistance measurements at room temperature also show a considerable resistivity enhancement between 2.4 and 3.8 GPa [36]. The resistance increase is expected to stem from the larger band gap for the intermediate phase [42]. Above 10.7 GPa, the resistance of the sample becomes detectable again, and it decreases with pressure, while the

R-T curves show weak temperature dependence. Metallization starts from 22.3 GPa, though the sample still shows some semiconducting features in the low-temperature range below 100 K. A sudden resistance dop is observed below 12 K at 23.9 GPa, suggesting a possible SC transition. Zero-resistance state is then observed at 26.4 GPa, and the SC transition is very sharp. Higher pressure suppresses the superconductivity as the T_c shifts to a lower temperature with pressure. The occurrence of metallization and the
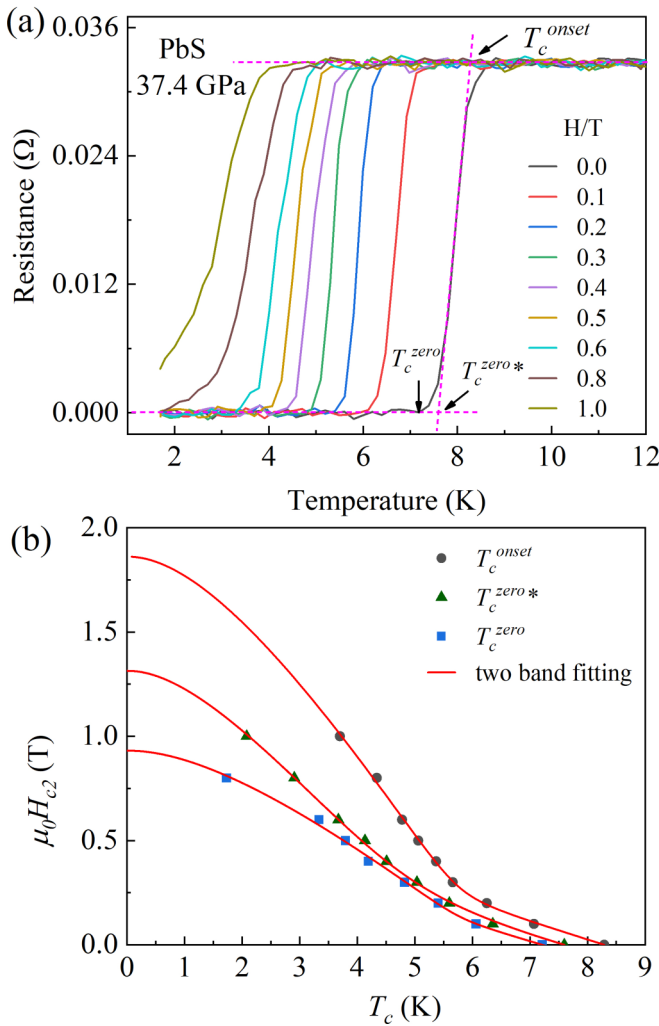
FIG. 3. The magnetic field effect on the superconducting transition in PbS crystal at 37.4 GPa and the relationship between the upper critical fields and SC transition temperature T_c. (a) The R-T curves near the SC transition at various magnetic fields; (b) the relationship plot of the upper critical magnetic field and T_c (T_c^{onset}, T_c^{zero*}, and T_c^{zero}), and the two-band model fitting.

following SC transition above 22.3 GPa is consistent with the orthorhombic-B2 cubic phase transition [34–36]. The R-T curves during decompression were also collected to check the stability of the SC state, and a higher T_c at 12.3 K is observed at 19.1 GPa. After that, the SC transition disappears, and the sample gradually returns to a semiconducting/insulating state.

The magnetic field effect further verifies the superconductivity, as presented in Fig. 3(a). At 37.4 GPa, the T_c is ∼8.3 K (as indicated by the arrow), and the external magnetic fields suppress the superconductivity, signaled by the T_c decline and broadening of the SC transition. Based on the R-T curves at various fields, the relation between the upper critical magnetic field and the T_c is plotted in Fig. 3(b). Unlike most binary metal sulfide SCs, the behavior of $\mu_0 H_{c2}$-T_c shows clear curvature behavior in the low magnetic field range, which is generally a feature of multiband superconductivity or anisotropic single-band superconductivity [43]. Similar

curvature behavior has been observed in MgB$_2$, YNi$_2$B$_2$C, and 2H−NbSe$_2$ [44,45], and they are typical multiband SCs. Since CsCl-type PbS crystallizes in a highly symmetric cubic structure, it is reasonable to assume the positive curvature behavior results from the multiband superconductivity, rather than the anisotropic single-band superconductivity. Currently, most multiband SCs are in the form of layered or highly anisotropic structures [43]. Therefore, CsCl-type PbS may represent a rare case of a cubic structure showing multiband SC features. Of course, more study is still required to confirm the multiband SC behavior, such as *in situ* high-pressure Andreev reflection spectroscopy characterization, which is beyond the scope of the current work. The curvature behavior was then fitted by the two-band model [43], giving $\eta = 5.16$, $D1 = 3.88$, and a zero-temperature upper critical field of $\mu_0 H_{c2} \approx 1.86$ T, when using T_c^{onset} as the fitting data, as seen in Fig. 3(b). The $\mu_0 H_{c2}$ is ∼1.31 T by fitting the H−T_c^{zero*} curve, and ∼ 0.93 T for H−T_c^{zero}. In pure sulfur, the zero-temperature upper critical field is estimated to be slightly higher than 1.7 T [10]. Here, a similar $\mu_0 H_{c2}$ (1.86 T) is observed in PbS, suggesting that the superconductivity is mainly contributed by the electrons from sulfur itself, as the critical field for Pb is quite low (less than 0.1 T) and the T_c of Pb is only ∼2 K at 20 GPa [46,47]. Meanwhile, we also note that the pressure suppresses the superconductivity in PbS, opposite to the pressure-enhanced SC in pure sulfur [11]. Therefore, Pb may be critical for superconductivity because Pb displays typical negative pressure-dependent SC behavior [47]. The electronic band structure calculation demonstrates that S contributes more electrons at the Fermi level rather than Pb, as seen in Fig. 4, which may reveal the origin of superconductivity in PbS, and verify the assumption of S-dominated superconductivity. Meanwhile, it is found that the DOS of S atoms decreases with pressure, and it could explain the negative pressure dependence of T_c to some extent. However, further theoretical calculations are still required to reveal the correlation between Pb and S, and the electron-phonon coupling behavior, which will provide a much clearer picture to understand the SC behavior in PbS. For the SC in 2H−TaS$_2$ and 2H−MoS$_2$ with a T_c higher than 10 K, the zero-temperature upper critical field is 1.1 T for the SC-II phase of TaS$_2$, and 7.5–8.1 T for MoS$_2$ [21,22]. Thus, the SC mechanism of PbS may be similar to the SC-II phase of TaS$_2$ (where the SC is dominated by sulfur itself), unlike MoS$_2$, in which Mo plays a critical role in forming Cooper pairs. Such an assumption is supported by the linear plot of the T_c-P relationship among PbS, 2H-TaS$_2$, and pure sulfur, as shown in Fig. 1, whereas 2H-MoS$_2$ is far from the line. This linear behavior also validates our initial motivation of precompressing sulfur by a metal. PbS becomes the first binary metal sulfide with a T_c higher than 10 K at moderate pressure.

While previous works mainly focus on the structural phase transitions under pressure, the optical behavior of the NaCl-type phase and the intermediate phase of PbS is rarely studied by *in situ* experiments. Here, by employing UV-VIS-NIR and infrared spectroscopies, we obtained the absorption and reflectance information of PbS, as presented in Fig. 5. The NaCl-type PbS is a small band gap semiconductor, and the initial band gap is ∼0.42 eV [41], which is consistent
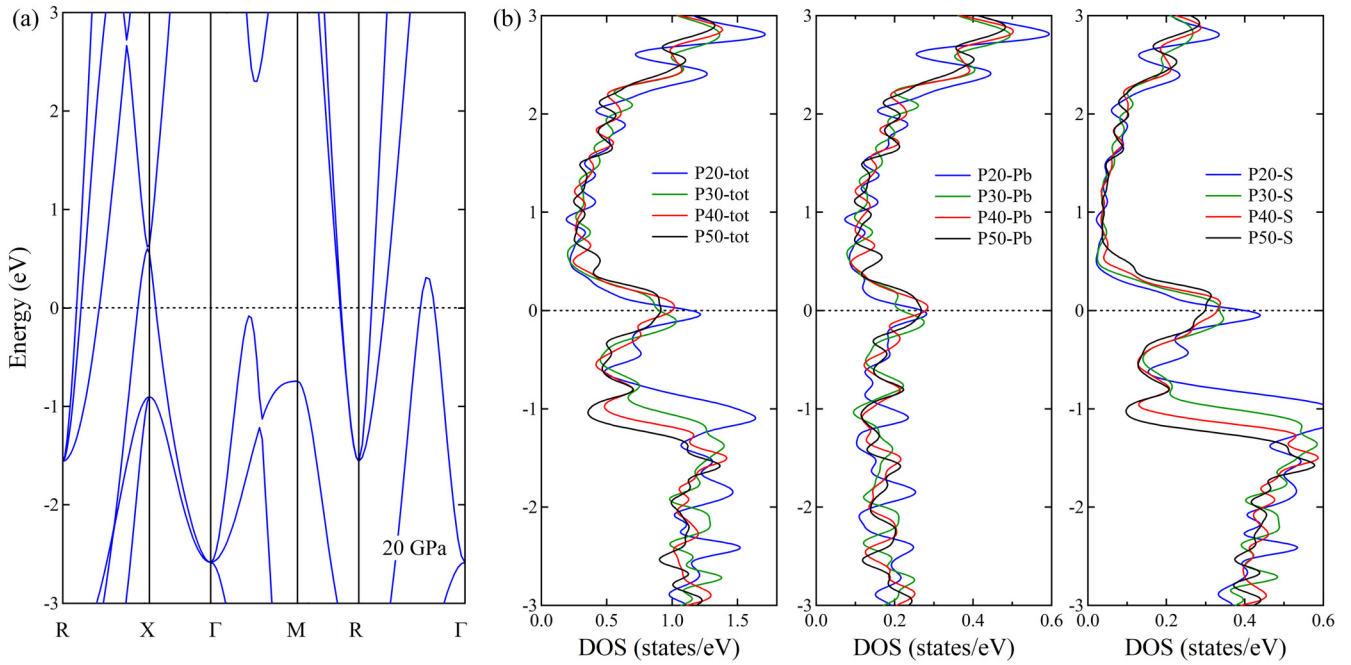
FIG. 4. Electronic band structure and density of states (DOS) for B2-type high-pressure PbS phase. (a) Electronic band structure under 20 GPa. (b) Total and partial density of states under 20, 30, 40, and 50 GPa.

with our optical measurement, as shown in Figs. 5(a) and 5(e). The pressure suppresses the band gap, and it is only ~0.2 eV near 2.5 GPa, above which PbS starts to transform

to the intermediate phase, accompanied by a much larger band gap of ~0.81 eV. Meanwhile, the sharp absorption edge of the NaCl-type phase disappears, replaced by a marginally wider
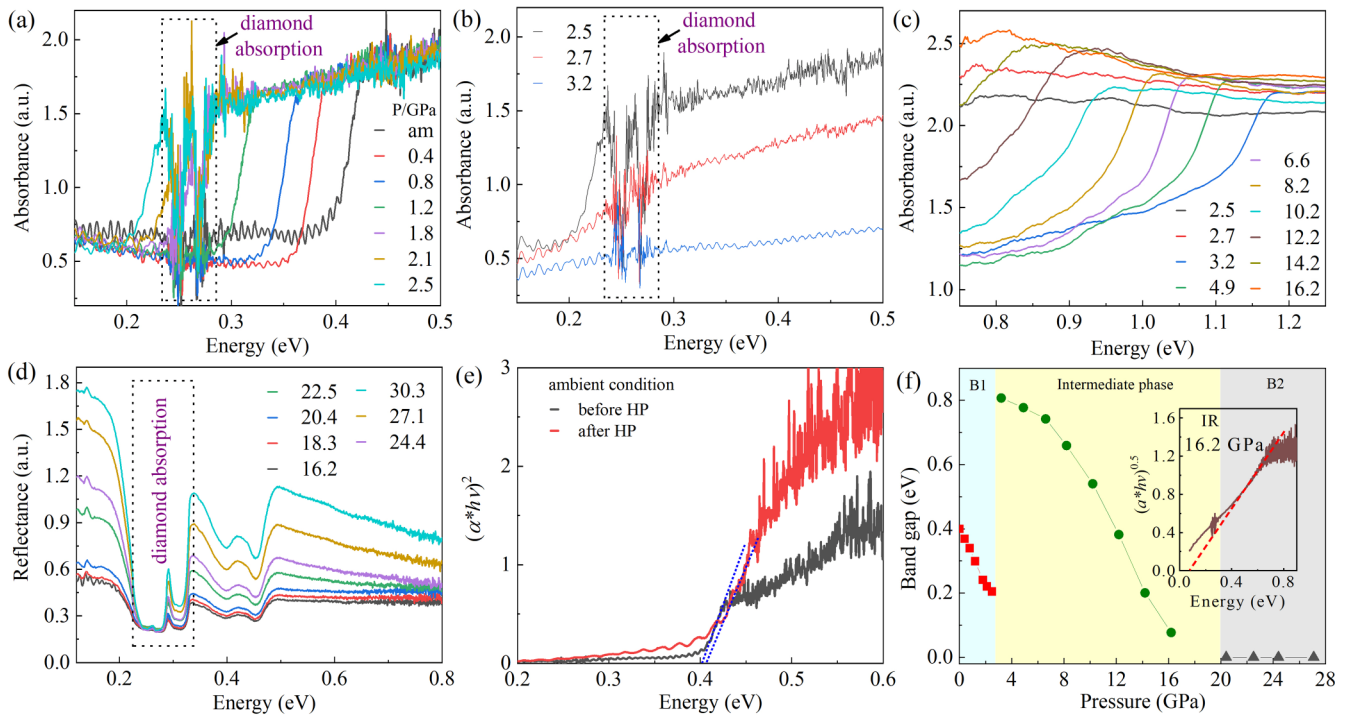

FIG. 5. The optical absorption and reflection spectroscopy for PbS under high pressure. (a) The infrared (IR) absorption spectra collected from ambient condition (am) to 2.5 GPa; (b) infrared absorption spectra collected during the B1-intermediate structure phase transition; (c) the UV-VIS-NIR spectra collected from 2.5 to 16.2 GPa; (d) infrared reflection spectra from 16.2 to 30.3 GPa; (e) the optical band gap fitting for ambient condition and recovered sample after high pressure; (f) the pressure-dependent optical band gap; inset: the band gap extracted from the IR data at 16.2 GPa.
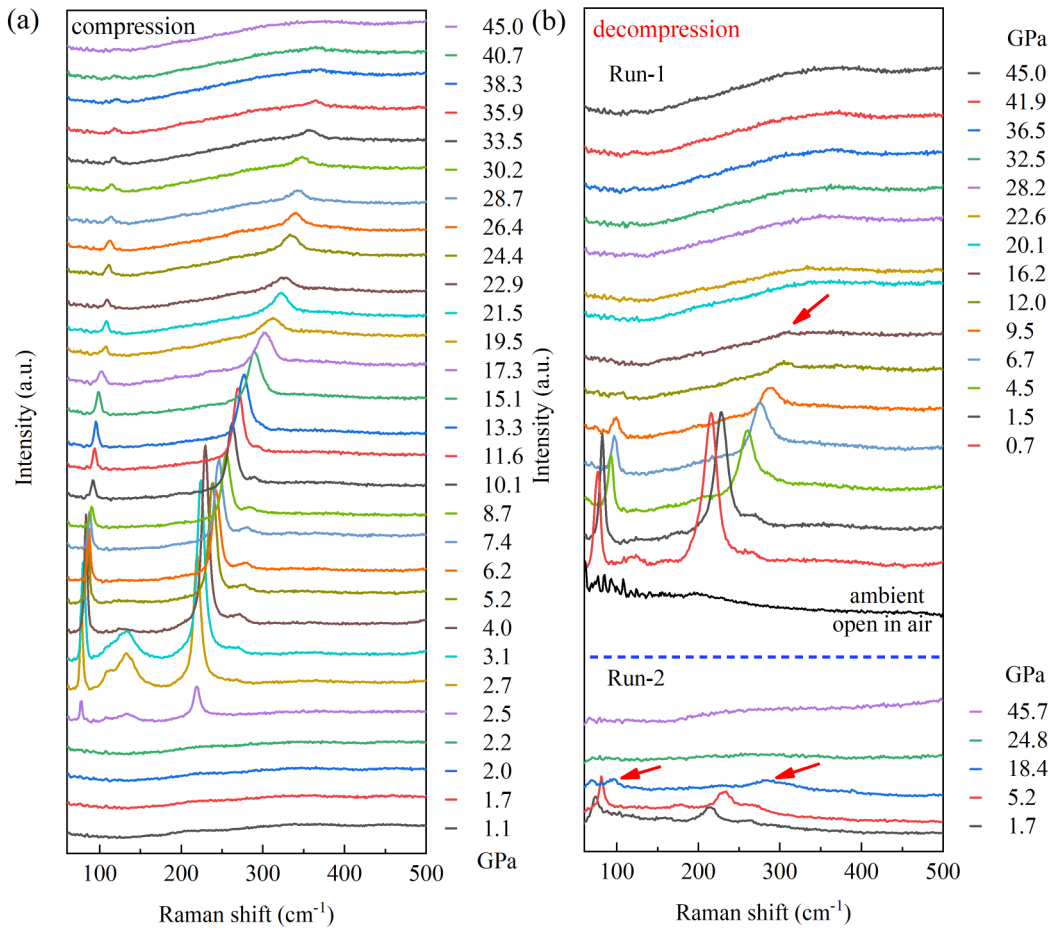
FIG. 6. The Raman spectra of PbS under high pressure. (a) The Raman data collected during compression; (b) the Raman data collected during decompression; red arrows show the Raman signal during the B2-intermediate structure phase transition. After fully releasing pressure, the sample returns to the original NaCl-type phase.

absorption edge, as shown in Figs. 5(a)–5(c), suggesting a transition from a direct band gap to an indirect band gap, as predicted by theoretical calculations [42]. For the intermediate phase, the external pressure also suppresses the band gap as the absorption edge gradually moves towards lower energy, as shown in Figs. 5(c) and 5(f). The metallization process is observed by measuring the reflectance spectra of PbS from 16.2 to 30.3 GPa, as displayed in Fig. 5(d). At 16.2 GPa, there is a clear interference signal below 0.2 eV, which becomes much weaker at 18.3 and 20.4 GPa, and becomes invisible above 22.5 GPa while the reflectance increases significantly. The interference signal's disappearance and the reflectance enhancement are typical metallization features. The above optical anomalies and transitions are consistent with previous structural studies and the electrical transport measurement in this work too.

The critical pressures for the structural phase transition can be well defined by the Raman signal evolution, as shown in Fig. 6. The Raman signal is extremely weak and almost undetectable for the NaCl-type phase due to the thermally activated metalliclike behavior at room temperature. Near 2.5 GPa, the Raman signal suddenly becomes strong, suggesting the appearance of an intermediate phase, as seen in Fig. 6(a). The intermediate phase lasts until 40.7 GPa. The phase transition from the intermediate phase to the CsCl-type

phase (B2 phase) is well studied, and the critical pressure is expected to be around 21.1–23 GPa [34–36]. The Raman signal above the critical pressure suggests a partial intermediate phase coexisting with the B2 phase, which is reasonable for a first-order structural phase transition. At 45 GPa, there is no clear Raman signal anymore. When the pressure is released, the critical pressure for the B2 phase–intermediate phase is between 20.1 and 18.4 GPa, as seen in Fig. 6(b), which is consistent with the transport measurement [as seen in Fig. 2(c)]. The critical pressure for the intermediate phase–B1 phase is below 0.7 GPa.

Based on the electrical transport results and structural evolution of PbS under pressure, a brief phase diagram is proposed in Fig. 7. During the compression process, the B1 phase of PbS behaves like a small band gap semiconductor (Semi-I). Then it transforms to a more insulating state (Semi-II) due to the larger band gap of the intermediate phase that appears above 2.5 GPa, as shown in Fig. 7(a). External pressure suppresses the band gap of the intermediate phase and enhances the conductivity. Further compression forces the transition from the intermediate phase to the B2 phase, which occurs near 22.3 GPa. PbS in the cubic B2 phase is metal and becomes a superconductor starting from 23.9 GPa at low temperatures. A relatively high $T_c > 12$ K is observed in the B2 phase, while the T_c shows quasilinear negative
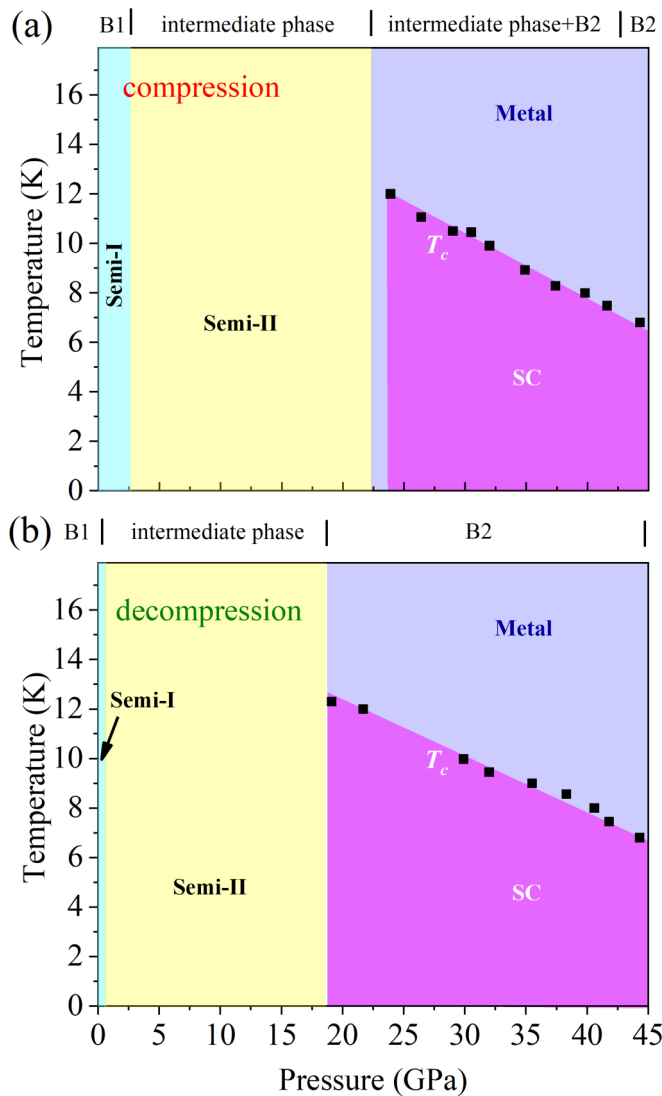
FIG. 7. Proposed brief phase diagram based on the electrical transport measurement and structural evolution under high pressure. The upper (a) and lower (b) panels correspond to the compression and decompression phase diagrams, respectively. Semi: semiconductor; SC: superconductor.

pressure dependence. During the decompression process, a higher $T_c \approx 12.3$ K is observed at 19.1 GPa, while the critical pressures of the above two transitions shift to lower pressures, as seen in Fig. 7(b).

IV. CONCLUSION

In summary, the electrical transport properties of a typical metal sulfide, PbS, were investigated under pressure. Superconductivity was observed in the high-pressure cubic phase of PbS above 23.9 GPa, and it showed a high T_c with possible multiband features. Furthermore, the external pressure suppressed the superconductivity and the highest $T_c \approx 12.3$ K was observed at 19.1 GPa during pressure release. This work shows a new metal sulfide superconductor with high T_c at moderate pressure. It also provides a simple alternative material system (both the structure and element components) to study the superconductivity mechanism, and is potentially beneficial for the study of multiband superconductors.

[1] K. Shimizu, Phys. C (Amsterdam, Neth.) **552**, 30 (2018).

[2] J. Hamlin, Phys. C (Amsterdam, Neth.) **514**, 59 (2015).

[3] K. Shimizu, Phys. C (Amsterdam, Neth.) **514**, 46 (2015).

[4] N. W. Ashcroft, Phys. Rev. Lett. **21**, 1748 (1968).

[5] E. Babaev, A. Sudbø, and N. Ashcroft, Nature (London) **431**, 666 (2004).

[6] S. A. Bonev, E. Schwegler, T. Ogitsu, and G. Galli, Nature (London) **431**, 669 (2004).

[7] M. I. Eremets, A. P. Drozdov, P. Kong, and H. Wang, Nat. Phys. **15**, 1246 (2019).

[8] X. Liu, P. Jiang, Y. Wang, M. Li, N. Li, Q. Zhang, Y. Wang, Y.-L. Li, and W. Yang, Phys. Rev. B **105**, 224511 (2022).

[9] C. Zhang, X. He, C. Liu, Z. Li, K. Lu, S. Zhang, S. Feng, X. Wang, Y. Peng, Y. Long, R. Yu, L. Wang, V. Prakapenka, S. Chariton, Q. Li, H. Liu, C. Chen, and C. Jin, Nat. Commun. **13**, 5411 (2022).

[10] S. Kometani, M. I. Eremets, K. Shimizu, M. Kobayashi, and K. Amaya, J. Phys. Soc. Jpn. **66**, 2564 (1997).

[11] V. V. Struzhkin, R. J. Hemley, H.-K. Mao, and Y. A. Timofeev, Nature (London) **390**, 382 (1997).

[12] E. Gregoryanz, V. V. Struzhkin, R. J. Hemley, M. I. Eremets, H.-k. Mao, and Y. A. Timofeev, Phys. Rev. B **65**, 064504 (2002).

[13] A. Drozdov, M. Eremets, I. Troyan, V. Ksenofontov, and S. I. Shylin, Nature (London) **525**, 73 (2015).

[14] A. Drozdov, P. Kong, V. Minkov, S. Besedin, M. Kuzovnikov, S. Mozaffari, L. Balicas, F. Balakirev, D. Graf, and V. Prakapenka, Nature (London) **569**, 528 (2019).

[15] M. Somayazulu, M. Ahart, A. K. Mishra, Z. M. Geballe, M. Baldini, Y. Meng, V. V. Struzhkin, and R. J. Hemley, Phys. Rev. Lett. **122**, 027001 (2019).

[16] F. Hong, L. Yang, P. Shan, P. Yang, Z. Liu, J. Sun, Y. Yin, X. Yu, J. Cheng, and Z. Zhao, Chin. Phys. Lett. **37**, 107401 (2020).

[17] R. Matsumoto, P. Song, S. Adachi, Y. Saito, H. Hara, A. Yamashita, K. Nakamura, S. Yamamoto, H. Tanaka, T. Irifune, H. Takeya, and Y. Takano, Phys. Rev. B **99**, 184502 (2019).

[18] X. Lai, Y. Liu, X. Lü, S. Zhang, K. Bu, C. Jin, H. Zhang, J. Lin, and F. Huang, Sci. Rep. **6**, 31077 (2016).

[19] X. Lai, H. Zhang, Y. Wang, X. Wang, X. Zhang, J. Lin, and F. Huang, J. Am. Chem. Soc. **137**, 10148 (2015).

[20] L.-C. Chen, H. Yu, H.-J. Pang, B.-B. Jiang, L. Su, X. Shi, L.-D. Chen, and X.-J. Chen, J. Phys.: Condens. Matter **30**, 155703 (2018).

[21] Z. Chi, X. Chen, F. Yen, F. Peng, Y. Zhou, J. Zhu, Y. Zhang, X. Liu, C. Lin, S. Chu, Y. Li, J. Zhao, T. Kagayama, Y. Ma, and Z. Yang, Phys. Rev. Lett. **120**, 037002 (2018).

[22] Q. Dong, J. Pan, S. Li, Y. Fang, T. Lin, S. Liu, B. Liu, Q. Li, F. Huang, and B. Liu, Adv. Mater. **34**, 2103168 (2021).

[23] V. G. Tissen, M. R. Osorio, J. P. Brison, N. M. Nemes, M. García-Hernández, L. Cario, P. Rodière, S. Vieira, and H. Suderow, Phys. Rev. B **87**, 134502 (2013).

[24] B. Yue, W. Zhong, W. Deng, T. Wen, Y. Wang, Y. Yin, P. Shan, J.-T. Wang, X. Yu, and F. Hong, J. Am. Chem. Soc. **145**, 1301 (2023).

[25] S. Nagata and T. Atake, J. Therm. Anal. Calorim. **57**, 807 (1999).

[26] D. C. Johnston and A. Moodenbaugh, Phys. Lett. A **41**, 447 (1972).

[27] Y. Ishihara and I. Nakada, Solid State Commun. **42**, 579 (1982).

[28] B. Yue, W. Zhong, X. Yu, and F. Hong, Phys. Rev. B **105**, 104514 (2022).

[29] L. F. Shi, Z. Y. Liu, J. Li, X. X. Zhang, N. N. Wang, Q. Cui, K. Y. Chen, Q. Y. Liu, P. T. Yang, J. P. Sun, B. S. Wang, Y. Uwatoko, Y. Sui, H. X. Yang, and J. G. Cheng, Phys. Rev. Mater. **6**, 014802 (2022).

[30] Y. Fang, J. Pan, D. Zhang, D. Wang, H. T. Hirose, T. Terashima, S. Uji, Y. Yuan, W. Li, and Z. Tian, Adv. Mater. **31**, 1901942 (2019).

[31] M. Izumi, T. Nakayama, K. Uchinokura, R. Yoshizaki, and E. Matsuura, Mol. Cryst. Liq. Cryst. **121**, 79 (1985).

[32] M. Monteverde, J. Lorenzana, P. Monceau, and M. Núñez-Regueiro, Phys. Rev. B **88**, 180504(R) (2013).

[33] K. Knorr, L. Ehm, M. Hytha, B. Winkler, and W. Depmeier, Eur. Phys. J. B **31**, 297 (2003).

[34] Y. Li, C. Lin, J. Xu, G. Li, X. Li, and J. Liu, AIP Adv. **4**, 127112 (2014).

[35] P. Bhambhani, N. Munjal, G. Sharma, V. V. Vyas, and B. K. Sharma, J. Phys.: Conf. Ser. **377**, 012068 (2012).

[36] J. Jiang, L. Gerward, R. Secco, D. Frost, J. Olsen, and J. Truckenbrodt, J. Appl. Phys. **87**, 2658 (2000).

[37] Y. Timofeev, B. Vinogradov, and E. Yakovlev, Phys. Solid State **23**, 1474 (1981).

[38] G. Kresse and J. Furthmüller, Phys. Rev. B **54**, 11169 (1996).

[39] P. E. Blöchl, Phys. Rev. B **50**, 17953 (1994).

[40] J. P. Perdew, A. Ruzsinszky, G. I. Csonka, O. A. Vydrov, G. E. Scuseria, L. A. Constantin, X. Zhou, and K. Burke, Phys. Rev. Lett. **100**, 136406 (2008).

[41] $PbS_{(1-x)}Se_{(x)}$ *Physical Properties, Datasheet from Landolt-Börnstein–Group III Condensed Matter, Vol. 41C: "Non-Tetrahedrally Bonded Elements and Binary Compounds I,"* edited by U. R. O. Madelung and M. Schulz (Springer-Verlag, Berlin, Heidelberg, 1998).

[42] S. Wang, J. Zhang, Y. Zhang, A. Alvarado, J. Attapattu, D. He, L. Wang, C. Chen, and Y. Zhao, Inorg. Chem. **52**, 8638 (2013).

[43] A. Gurevich, Phys. Rev. B **67**, 184515 (2003).

[44] H. Suderow, V. Tissen, J. P. Brison, J. L. Martinez, S. Vieira, P. Lejay, S. Lee, and S. Tajima, Phys. Rev. B **70**, 134518 (2004).

[45] A. Majumdar, D. VanGennep, J. Brisbois, D. Chareev, A. V. Sadakov, A. S. Usoltsev, M. Mito, A. V. Silhanek, T. Sarkar, A. Hassan, O. Karis, R. Ahuja, and M. Abdel-Hafiez, Phys. Rev. Mater. **4**, 084005 (2020).

[46] D. L. Decker, D. Mapother, and R. Shaw, Phys. Rev. **112**, 1888 (1958).

[47] B. Bireckoven and J. Wittig, J. Phys. E: Sci. Instrum. **21**, 841 (1988).